Biochimica et Biophysica Acta, 1121 (1992) 189–198

BBAPRO 34210

Structural fluctuations and conformational entropy in proteins: entropy balance in an intramolecular reaction in methemoglobin

Heinz-Jürgen Steinhoff, Jürgen Schlitter, Albrecht Redhardt, Dirk Husmeier and Norbert Zander

Institut für Biophysik, Ruhr-Universität Bochum, Bochum (Germany)

(Received 17 October 1991)

Key words: Hemoglobin; Heme binding; Temperature jump; Configurational entropy; Vibrational entropy

The reversible intramolecular binding of the distal histidine side chain to the heme iron in methemoglobin is of special interest due to the very large negative reaction entropy which overcompensates the large reaction enthalpy. It may be considered as a prominent example of the ability of proteins (including enzymes) to provide global entropy in a local process. In this work new experiments and model calculations are reported which aim at finding the structural elements contributing to the reaction entropy. Geometrical studies prove the implication of the 20 residue E-helix being shifted by more than 2 Å. Vibrational entropies are calculated by a procedure derived from the method of Karplus and Kushik. It turns out that neither the histidine alone nor the complete E-helix contribute more than 15 per cent of the required entropy.

Introduction

Fluctuations, especially structural fluctuations, are connected with the corresponding variable of state, the entropy, by fundamental physical principles [1]. The biological relevance of local and global fluctuations of the structure of macromolecules, e.g. proteins, has been proven in a couple of recent publications. Perutz has shown, for example, that the distal histidine in myoglobin occupies the role of a fluctuating barrier which influences or controls the exchange of O_2 with the environment [2]. Frauenfelder and co-workers observed abnormal temperature dependencies of the rms deviations of the atomic coordinates of proteins [3]. As a result the concept of conformational substates and fluctuating energy barriers has been developed [4,5]. Recent EPR measurements on the viscosity dependence of the fluctuations of protein-bound spin labels support this concept [6].

The entropy balances of these fluctuation processes were investigated in relation to their biological relevance in former studies too. Koshland [7] and Westheimer [8] considered the potentiality of the macromolecules in their enzymatic function to act as an entropy trap. In this context it is interesting to note that the value of the vibrational entropy of relative small proteins, e.g. bovine pancreatic trypsin inhibitor, is enormous as calculated by Brooks and Karplus 20 years later [9]. Page and Jencks [10] consider entropic contributions as an important driving force for enzymatic and intramolecular reactions. By means of detailed numerical entropy calculations the authors give an explanation for the factor 10^8 found for an effective molarity which characterizes the increase of the reaction rates for enzymatic reaction in relation to usual bimolecular reactions.

According to this it seems a fascinating project to relate the entropy change found in macromolecular reactions to fluctuation parameters. This problem seems to be attractive in particular because both parameters, entropy and fluctuations, have the same origin and, on the other side, they are determined by completely different methods: entropy changes are determined by the classical methods of experimental and theoretical physical chemistry [11]. Fluctuation parameters are studied by X-ray diffraction [3], Mössbauer spectroscopy [12], neutron scattering spectroscopy [13] and electron paramagnetic resonance [6] as well as theoretically by matrix techniques [14] and molecular dynamics simulations [15].

A comparison between entropy balance and fluctuation parameters appears to be successful especially for processes with dominating entropy fluxes. These are denaturation processes of proteins the vibrational en-

Correspondence: H.-J. Steinhoff, Institut für Biophysik, Ruhr-Universität Bochum, Universitätsstrasse 150, Postfach 102148, D-4630 Bochum, Germany

tropy of which is studied in harmonic approximation in Ref. 14 and is found to be an extensive function.

The present paper follows the ideas developed in Ref. 14 with regard to principle and numerical methods: the question of the vibrational part of the entropy of an entropy driven reaction is studied and compared to the results of an experiment. As in Ref. 14 the vibrational entropy is calculated in harmonic approximation and the method of numerical blocking of amino acid side chains is applied. The type of studied reaction, however, as well as the relation to the numerical model are different. In the present paper the reversible intramolecular binding reaction of N_ϵ of the distal histidine E7 to the heme iron of methemoglobin [16–18] is investigated. As well as the denaturation processes discussed in [14] this reaction is controlled in an exceptional extent by the entropy change. In contrast to protein denaturation we expect, however, that the intramolecular reaction is rather independent on solvent effects [10]. Additionally the intramolecular reaction may serve as a model reaction of enzymatic processes [19]. The reaction sketched above is studied experimentally by means of the temperature-jump technique, an improvement of the apparatus is described in appendix A.

We characterize the applied theoretical model as a 'realistic minimum model'. It is realistic because one helix (E-helix) is studied which is adjacent to the reaction site and one residue (histidine E7) is blocked which is fixed by the chemical binding reaction. The model is a minimum model because only this helix is studied and a harmonic approximation is applied. Movements within this helix must certainly be coupled to neighboring helices and non-helical regions in the vicinity. It will be discussed which fraction of the experimentally determined reaction entropy can be attributed to a reduced vibrational entropy of a restricted portion of the structure. A numerical method for the determination of the vibrational entropy is described in Appendix B.

Methods

Preparation of horse methemoglobin

Horse methemoglobin (metHb) was prepared similar to the procedure given in [20]. Fresh blood samples (carotid, healthy horse, 50 ml blood + 9 ml 3.2% sodium citrate), were prepared at 4°C throughout in all the following steps. The cell suspensions were centrifuged 15 min at $2440 \times g$, then washed three times with 0.9% NaCl solutions and hemolyzed by addition of equal amounts of destilled water. For separating the membranes, solid NaCl was added, leading to 5% NaCl concentration in the suspension and then centrifuged 1 h at $30000 \times g$. Organic phosphates were removed by dialyzing overnight against 50-fold of 0.1 M phosphate buffer (pH 7.4). Two further dialysis steps were done using the same buffer for 30 min and 0.1 M phosphate buffer (pH 6.8) for 1 h. For oxidation to methemoglobin the 2-fold stoichiometric amount of $K_3(Fe(CN)_6)$ was added carefully in solution. The sample was desalted by running through a Sephadex G25, length 60 cm, eluted with 0.1 M phosphate buffer (pH 6.8). Finally the samples were filtered with millipore, pore diameter 1.2 μm. Two types of sample were then used for the measurements: samples prepared every week and used during this week. Larger amounts of samples were frozen in Eppendorf polyethylene samples holders at 77 K, stored up to 4 weeks at −12°C and thawed before measurement in a waterbath at 4°C. Methemoglobin concentrations were determined after reaction with CN^- using the optical extinction coefficient $\epsilon_{540nm} = 11500$ l/(mol cm).

Temperature-jump measurements

The temperature-jump measurements aim on the determination of the thermodynamic data of the reaction shown in Fig. 1 and analysed physicochemically in Ref. 16–18. Especially the precise determination of the reaction entropy ΔS requires essential improvements of the apparatus and the experimental procedure in relation to Refs. 16 and 17. The temperature-jump is performed in the usual way by the discharge of a condenser across the sample. The value of the achieved temperature-jump amplitude ΔT was calibrated optically by means of the determination of the extinction change of a buffered solution of Kresol red with known temperature coefficient. Additionally the electrical energy which is converted into heat within the sample was determined from the time-course of the current $I(t)$ through the sample cell and the voltage $U(t)$ at the cell electrodes using a fast multiplier (Philbrick, 4457) joint with an integrator. Certain components of the apparatus have been adapted to the special reaction observed here so that the signal to noise ratio has been improved 10-fold compared to the experiments discussed in Refs. 16–18. The monochromator has been replaced by interference filters ($\lambda = 420$ nm, $\Delta\lambda = 9$ nm; $\lambda = 633$ nm, $\Delta\lambda = 12$ nm) and photodiodes (BPW 34, BPW 21) are used instead of a photomultiplier. The thermodynamic data are deduced from the amplitude of the extinction change ΔE after the temperature-jump. A simple and precise method has been developed to determine the absolute value of ΔE (cf. Appendix A). Extinction values E between 0.6 and 0.7 were employed for the measurements according to methemoglobin concentrations of 0.4 mM for $\lambda = 633$ nm and 40 μM for $\lambda = 420$ nm.

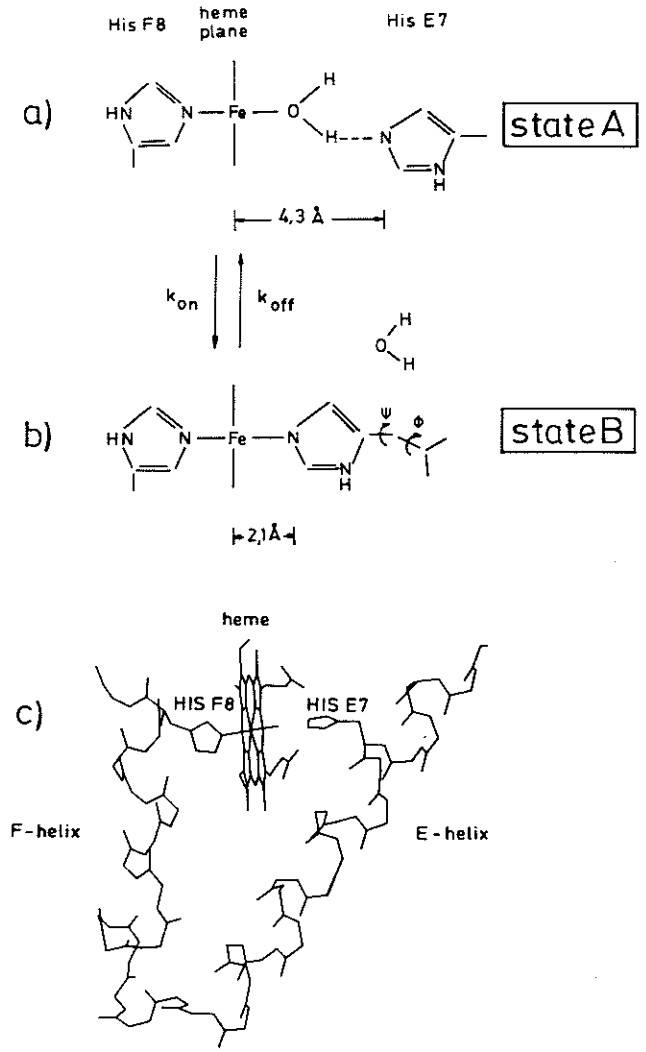

Fig. 1. Heme area of methemoglobin A, α-chain, and reaction scheme. (a) State A and (b) state B. With ψ we designate the dihedral rotation angle next to the imidazole ring, Φ denotes the other C–C rotation angle (c) View of the heme area with adjacent helices E and F.

The analysis of the relaxation transients follows the procedure discussed in [17]. The reaction shown in Fig. 1 can be written as:

$$A \rightleftharpoons B \tag{1}$$

The time-course of the extinction of the sample that follows a temperature-jump is given by

$$E(t) = E_0 + \Delta E(1 - e^{-t/\tau}) \tag{2}$$

The relaxation time τ for the reaction (1) is

$$\tau^{-1} = k_{on} + k_{off} \tag{3}$$

where k_{on} and k_{off} are the rate coefficients of the association and dissociation of the N_ϵ of the distal histidine to and from the iron atom. The equilibrium constant K is defined as

$$K = [B]/[A] = k_{on}/k_{off} = \exp\{-\Delta H^0/RT + \Delta S^0/R\} \tag{4}$$

The reaction enthalpy ΔH^0 and reaction entropy ΔS^0 are related to the experimental value ΔE by [17,18,21]

$$K = \frac{(1-V)Y}{2XT^2} + \left\{\left[\frac{(1-V)Y}{2XT^2}\right]^2 + V\right\}^{1/2} \tag{5}$$

and

$$\Delta H^0 = RY\frac{(K+1)(K+V)}{K^2 - V} \tag{6}$$

where $X(\lambda, T) = \Delta E/(E\Delta T)$, $Y = \mathrm{d}\ln(|X|T^2)/\mathrm{d}(T^{-1})$. V is the ratio of the extinction coefficients of A and B, $\varepsilon_A/\varepsilon_B$. We use $V_{\lambda=420\text{ nm}} = 0.68$ and $V_{\lambda=633\text{ nm}} = 3.0$ [17]. In the temperature range investigated here the limit $K \ll 1$ holds and Eqns. 3 and 6 may be simplified:

$$\tau^{-1} = k_{off} \tag{7}$$

$$\Delta H^0 = -RY \tag{8}$$

Activation quantities are calculated according to the relation of Eyring

$$k_{off} = kT/h \exp\{-\Delta G^\ddagger/RT\} \tag{9}$$

where

$$\Delta G^\ddagger = \Delta H^\ddagger - T\Delta S^\ddagger \tag{10}$$

Model calculations

For both reaction states a dynamical model was designed in order to obtain numerical estimates of the reaction entropy. The reaction states A and B sketched in Fig. 1a and 1b were modeled by dynamical states of the E-helix including the side chain His E7 immediately involved in the reaction. For the sake of simplicity the model states were named A and B, too. The model thus aimes merely at estimating the contribution of that part of the protein.

At a given temperature the classical entropy of a system is a measure of the atomic fluctuations and their mutual correlations which are both determined by the underlying force field. In our model calculations we use the GROMOS force field [22] and confined ourselves to internal vibrational motions of the E-helix i.e., to harmonic dynamics. The isolated E-helix was energy minimized by means of a GROMOS routine using conjugate gradients. Final convergence was accomplished and checked by a special method using the

Hessian matrix of second derivatives [23]. The resulting coordinate set was the starting point for generating several dynamical model states which all (except B_1, see below) allow vibrations about these coordiantes of minimum energy. They differ, however, by certain restrictions imposed to the dynamics which are modelling the influence of the remainder of the protein and, in state B, the effect of the bond created in the reaction.

State A. Starting from the known X-ray coordinates of horse methemoglobin [24] the isolated E-helix was energy minimized until a residual gradient of 0.7 kJ mol^{-1} Å^{-1} was reached. The final rms-deviation from the X-ray structure was 1.2 Å. We then considered two dynamical states of the helix: A_1 designates the state where all atoms, in particular the interesting side chain His E7, are free to move about the minimum structure. In state A_2 three backbone atoms at the helix ends were fixed in order to model the fact that the helix is actually part of a larger molecule. Both dynamical states are reasonable models of the initial state A where N_ε of His E7 is not yet bound to the heme iron.

State B. Modelling the final state by a dynamical state of the E-helix requires an idea as to how the mobility of the ligand His E7 is restricted by the bond to the heme iron. As both transitional and rotational degrees of freedom are expected to be more or less reduced, we used several dynamical states as possible models:

B_1 is a dynamical state of the free helix like A_1, but with blocked torsion angles Φ and ψ, see Fig. 1b. The angles are kept at their X-ray values, which requires an additional energy minimization with a restraint potential. The resulting distance in configurational space between A_1 and B_1 is $\delta = 0.29$ Å.

B_{21}–B_{25} are dynamical states of the fixed helix like A_2. They differ from A_2 by blocking of one or several of the following motions: translation of N_ε, rotation about Φ, and rotation about ψ. In each case the force field was modified by an appropriate additional restraint term which, however, did not change the mean structure relative to A_2.

For estimating entropy differences in our dynamical model states we consider the vibrations about a mean structure of minimum potential energy. The E-helix consists of 173 heavy atoms and charged hydrogens. The calculations were performed with the GROMOS force field and programs and special routines for accelerated minimization and the evaluation of the vibrational entropy (see Appendix).

For blocking a coordinate ξ at a value ξ_0 and for fixing the helix ends we used a harmonical restraint potential $V_r = 0.5\ \kappa\ (\xi - \xi_0)^2$. The force constant κ was increased until the entropy reached a stationary limiting value. Due to the strong restraint potential high-frequency modes are produced which require a quantum mechanical calculation of the entropy. The procedure given in the appendix is closely related to the method in Ref. 25.

Results and Discussion

Experiments

A typical transient record after a temperature-jump of 3.2 K is shown in Fig. 2. Relaxation amplitude ΔE and relaxation times τ are determined from least-squares fitting procedures of single exponentials to the experimental transients. Thermodynamic and kinetic parameters are calculated from these experimental data as described in the Methods. They are shown in Table I. The observed reaction is interpreted in terms of the scheme shown in Fig. 1 for the reasons given in [17]. In state A we have H_2O as ligand of the heme iron, in state B the N_ε of the distal histidine E7 is the sixth ligand of the iron, the H_2O molecule being displaced. If we consider the X-ray coordinates of the histidine residue E7 and the iron atom as a first approximation of the time average of the coordinates in aqueous solution the binding reaction shown in Fig. 1 is possible only if the distance r between N_ε and Fe is lowered by nearly 0.2 nm. Thus, the reaction can only occur if the E-helix and the heme carry out thermal fluctuations relative to each other with amplitudes of the order of the required distance reduction of 0.2 nm (this will be discussed in detail in the next section).

The values of the reaction enthalpy and entropy are in good agreement with earlier work [17], the margin of errors has been lowered. Despite of the large difference between the temperature intervals under investigation the values of the reaction enthalpy and entropy

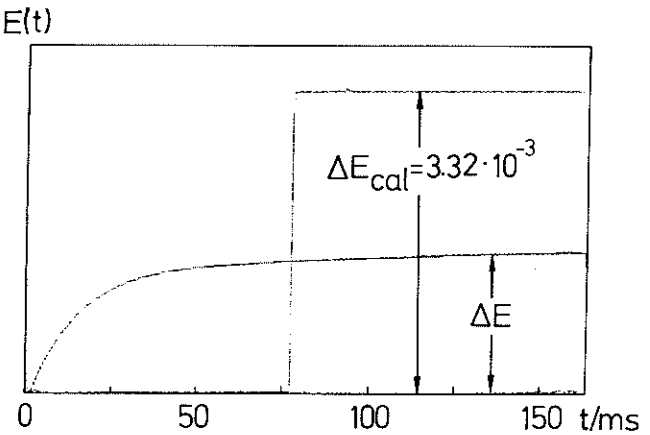

Fig. 2. Time-course of the extinction change after a temperature-jump of $\Delta T = 3.2$ K at 274 K in $4 \cdot 10^{-4}$ M methemoglobin solution, $E = 0.63$, pH 6, $\lambda = 633$ nm. The calibration mark is generated as described in Appendix A. The difference between the experimental curve and a fitted single exponential is enhanced by a factor ten and shown as a series of points near the abscissa. The relaxation amplitude and the relaxation time taken from the fitting procedure are $\Delta E = 1.6 \cdot 10^{-3}$ and $\tau = 17.5$ ms. Extinction noise is less than $0.5 \cdot 10^{-5}$.

TABLE I

Equilibrium and relaxation data from temperature-jump measurements of aqueous methemoglobin solutions, pH 6

$[(NH_4)_2SO_4]$/mol	0	0.1	0.3	0.5	1
ΔH^0/kJ mol^{-1}	−68	−70	−66	−69	−67
ΔS^0/J mol^{-1} K^{-1}	−284	−284	−270	−277	−268
ΔG^0/kJ mol^{-1}	16.5	14.6	14.2	14.0	13.2
$K/10^3$ (T = 298 K)	1.3	2.8	3.3	3.4	4.8
$\Delta H^\ddagger$/kJ mol^{-1}	87	91	92	92	91
$\Delta S^\ddagger$/J mol^{-1} K^{-1}	112	119	129	127	131
$\Delta G^\ddagger$/kJ mol^{-1}	54	54	54	54	54
k_{off} (298 K)/10^3 s^{-1}	2.1	2.1	2.1	2.1	2.1
k_{on} (298 K)/s^{-1}	2.7	5.9	6.9	7.1	8.2

[metHb] = 40 μM heme; buffer concentration $[Na_2HPO_4]$ = 86 mM; $[NaH_2PO_4]$ = 9.4 mM. The standard deviations σ are: $\sigma(\Delta H^0)$ = 2 kJ/mol; $\sigma(\Delta S^0)$ = 10 J/(mol K); $\sigma(\Delta G^0)$ = 2 kJ/mol; $\sigma(\Delta H^\ddagger)$ = 2 kJ/mol; $\sigma(\Delta S^\ddagger)$ = 8 J/(mol K); $\sigma(\Delta G^\ddagger)$ = 2 kJ/mol. The data of k_{off} and $\Delta G^\ddagger$ are directly taken from the time-course of the extinction change (cf. Fig. 2) at T = 298 K, the activation entropy and enthalpy are taken from plots of log τ vs. T^{-1} according to Eqns. 9 and 10.

shown in Table I coincide within experimental errors with those for the protein frozen in solution. Using EPR methods ΔH^0 and ΔS^0 have been determined in a temperature range between 255 K and 235 K [26], $\Delta H^0 = (-82 \pm 10)$ kJ/mol, $\Delta S^0 = (-333 \pm 41)$ J mol^{-1} K^{-1}. Thus, freezing of bulk water in methemoglobin solutions does not prevent thermal fluctuations of the required amplitude and the reaction (Fig. 1) is observable. However, temperature-jump investigations of single crystals of methemoglobin confirm that the binding reaction (Fig. 1) cannot be observed in the crystallized phase of the protein within a time range of 100 s [27]. In these experiments the methemoglobin single crystals have been covered with mother liquor of high concentrations of $(NH_4)_2SO_4$ (2.2 M) or Na_2SO_4 (1.2 M). To determine the influence of these salts on the observed reaction the thermodynamic and kinetic parameters have been studied as a function of salt concentrations. The results for ammonium sulfate are shown in Table I. We note that the equilibrium constant K as well as the relaxation amplitude ΔE (cf. Eqn. 9) increase with increasing $[(NH_4)_2SO_4]$. This result is valid up to concentrations of ammonium sulfate where the protein precipitates. Thus the high ammonium sulfate concentration in the crystal mother liquor is not responsible for the absence of the reaction in single crystals and we have to conclude that crystallization prevents the N_ε of the distal histidine from binding to the iron.

The kinetic parameter k_{off} and therefore $\Delta G^\ddagger$ can be deduced from the relaxation transients with high accuracy. The independence of k_{off} and the increase of K imply that the binding probability of the N_ε to the iron atom increases with increasing ammonium sulfate concentration. The replacement of small amounts of water molecules at the sixth binding site of the iron by ammonia may possibly contribute to the observed change of K [28]. On the other side, a clear increase of K with increasing ionic strength was also observed in solutions with Na_2HPO_4 (86 mM $\leq c \leq$ 860 mM) or Na_2SO_4 (100 mM $\leq c \leq$ 500 mM). In these cases the increase of K with salt concentration amounts to 30–50% of the values observed with ammonium sulfate in similar concentration intervals.

We summarize the experimental results: The application of the simple procedure of absolute determination of optical relaxation amplitudes given in Appendix A enables us to use the classical temperature-jump method to determine precise thermodynamic data of biochemical reactions. The association rate k_{on} of the N_ε in the present reaction (Fig. 1) increases with increasing ionic strength. The effect is pronounced for ammonium sulfate solutions. This behavior is correlated with the decrease of the reaction entropy $\Delta S°$ (cf. Table I). According to this we conclude that the conformation of the methemoglobin molecule is influenced with increasing salt concentration in such a way that the probability for the N_ε of the distal histidine to 'find' the iron is increased. We would expect a decrease of k_{off} with increasing salt concentrations due to the altered water activity. In contrast to this the dissociation rate k_{off} and the activation free energy $\Delta G^\ddagger$ do not depend on $[(NH_4)_2SO_4]$ within experimental error. The influence of the ionic strength on the protein structure mentioned above could be responsible for this behavior. The binding reaction is coupled with a large negative reaction entropy, $\Delta S \approx -280$ J mol^{-1} K^{-1}. For the equilibrium constant K we obtain

$$K_{298\,K} = [B]/[A] = \exp\{-\Delta H^0/RT\} \exp\{\Delta S^0/R\}$$

$$= 8.3 \cdot 10^{11} \cdot 1.5 \cdot 10^{-15} = 1.2 \cdot 10^{-3}$$

so that state A with the distal histidine not bound to the iron is favoured at physiological temperatures. The very large exothermic enthalpy term is overcompensated by a still larger value of the entropy term. This result justifies the application of the discussed reaction as a model for a quantitative study of intramolecular entropy fluxes.

Model calculations

The geometry of the reaction site displayed in Fig. 1 shows that the nitrogen N_ε of the histidine His E7 must be shifted about 2 Å in order to reach the correct bond distance to the heme iron. First one may ask if the shift can arise from motions in the residue alone, i.e., by variation of the torsion angles Φ and ψ shown in Fig. 1b. We, therefore, calculated the distance $d = d(\mathrm{Fe} - N_\varepsilon)$ for different Φ and ψ using the X-ray coordinates [24]. The result is shown in Fig. 3. The

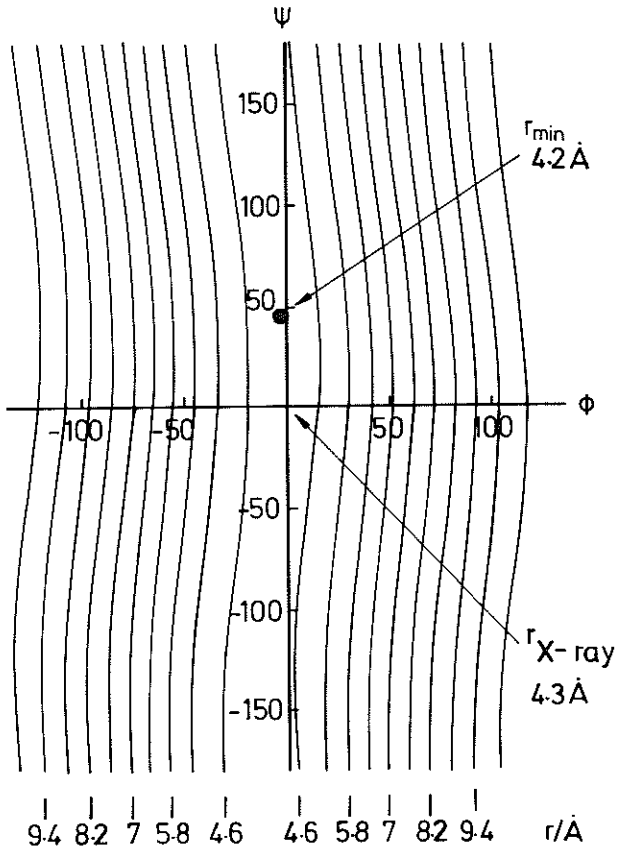

Fig. 3. Distance Fe–N_ε (His E7) as a function of the dihedral angles Φ and ψ (see Fig. 1). The minimum distance is 4.2 Å (filled circle). The origin $\Psi = \Phi = 0$ corresponds to the geometry found in the crystal structure with $d = 4.3$ Å.

origin $\Phi = \psi = 0$ with distance $d = 4.3$ Å corresponds to the geometry found in the crystal structure. By a relatively small variation of Φ and ψ a slightly smaller minimum distance $d_{min} = 4.2$ Å can be produced. The gain of 0.1 Å is negligible compared with the required shift towards the bond distance of 2.1 Å. Thus, obviously a reorientation of the residue itself is not sufficient to bring about the necessary shift of the N_ε.

We conclude, therefore, that a conformational change of the protein connected with a considerable relative motion of the heme and the E-helix is required for the internal bond to be closed. Together with the rate constants in Table I, this leads to the following picture: At room temperature the bond N_ε–Fe is open for about 0.5 s with the tertiary structure performing considerable fluctuations. The amplitudes of the fluctuations of the distance d can go up to 2 Å. Once the sterical requirement being satisfied, the energetically favoured bond Fe–N_ε is closed. At room temperature it has a life time of about 0.5 ms before it is broken by thermal fluctuations.

However, the present dynamical model calculations are not intended to describe the gross fluctuations revealed by the occurence of the reaction. They rather aim at estimating the vibrational contribution to the reaction entropy effected by the E-helix, which is the largest element of the tertiary structure involved in the reaction. The model states hence comprise only the E-helix with the binding residue His E7. Foregoing estimations have shown that a further reduction to the histidine alone would make no sense.

In our model calculations on the isolated E-helix we had to allow for the fact that the helix in the protein is actually fixed by 'soft' geometrical boundary conditions. We considered two cases: a free helix and a helix with three fixed backbone atoms at the helix ends. As to the mobility of the helix as a whole in the protein, the model states A_1 (free helix) and A_2 (helix fixed at the ends) and their corresponding analogues of state B are marking the range of reasonable approximations for an entity being part of a protein. The unhindred fluctuation of all residues may result in too large an entropy, in particular for His E7 which in state A can have a H-bridge to the ligand water at the heme iron. (We note in passing that, in contrast to the crystal structure, the MD-simulation with solvent shows a rather loose H-bond (Schlitter, J. and Husmeier, D. unpublished)).

There is more freedom to define the final state of the E-helix. It is clear from the foregoing discussion of the geometry, that the mobility of His E7 (and hence of the whole helix) will be reduced by the bond Fe–N_ε which brings His E7 in contact with the massive heme group. When the effect of the reaction is studied at the free helix ($A_1 \rightarrow B_1$) one can only consider rotational immobilization of the histidine torsional angles. Here we blocked the angles at their X-ray values which were shown to practically minimize the distance of the reaction partners. The model of a fixed helix with initial state A_2 enables one to investigate also the effect of the fixation of the atom N_ε by the reaction. Together with the angle immobilizations we therefore consider five possible model transitions ($A_2 \rightarrow B_{2i}$).

One should bear in mind that in our model calulations different dynamical states of the E-helix are compared which, however, all possess the same mean structure, i.e., all coordinates have the same mean value in all states. The only exception is B_1 which was forced to assume special torsion angles. In all cases the motion of one or several variables was completely blocked in the final state, which gives too small an entropy. Because of the consistently overestimated entropy of state A, the present calculation hence gives an upper limit for the loss of vibrational entropy in the E-helix during the reaction. The definition of model states and results are summarized in Table II.

Free helix ($A_1 \rightarrow B_1$). This transition leads to a different point in the configurational space since the torsion angles Φ and ψ were blocked not at the values they had in A_1, but at their X-ray values which nearly

TABLE II

Transitions between model states and associated entropy differences

Model for state A	Blocked	Model for state B	ΔS (J/mol per K)
free helix			
	$\Phi\ \Psi$	$A_1 \rightarrow B_1$	-35.3
fixed helix			
	N_ε	$A_2 \rightarrow B_{21}$	-17.5
	Φ	$\rightarrow B_{22}$	-27.4
	Ψ	$\rightarrow B_{23}$	-27.4
	$\Phi\ \Psi$	$\rightarrow B_{24}$	-31.6
	$N_\varepsilon\ \Phi\ \Psi$	$\rightarrow B_{25}$	-34.4

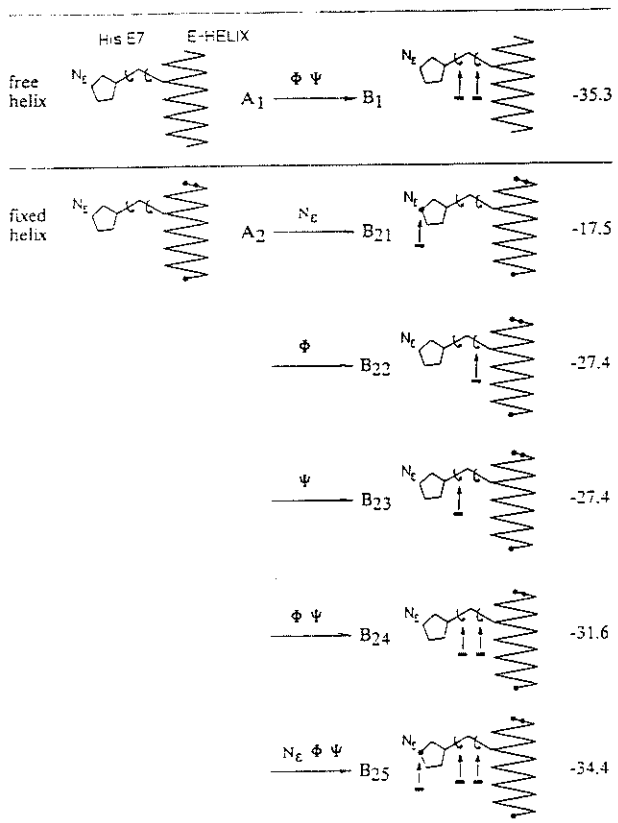

minimize the distance Fe–N_ε. The rms-shift is 0.92 Å, $\Delta S = -35.3$ J/mol per K. The new minimum energy is by 0.84 RT higher than in A_1, where RT is the thermal energy at 298 K. As in a similar investigation [14] there is no enthalpy/entropy compensation as ΔE and $-T\Delta S$ increase simultaneously.

Helix with fixed ends ($A_2 \rightarrow B_{2i}$). The model transitions starting at A_2 are performed by blocking different variables at the values they had in state A_2. Hence one has no rms-shift, and the entropy differences arise solely from the hindred motions in the final states modelling the effect of the bond Fe–N_ε. The least effect occurs when N_ε is blocked. Blocking Φ or ψ gives the same, much larger entropy difference. When all three degrees of freedom are suppressed one has $\Delta S = -34.4$ J/mol per K, which is somewhat less than in the free helix.

Comparing the results of our model calculations with different assumptions on the helix boundary conditions and the effect of the bond Fe–N_ε onto the dynamics of the E-helix, we can be shure to have calculated at least the order of magnitude of the contribution from vibrational entropy to the reaction entropy.

Comparison of experiment and theory

The new experiments presented in this work yield a reaction enthalpy and entropy which are in good agreement with earlier work [17]. Of highest interest is the large negative reaction entropy ($\Delta S \approx -280$ J/mol per K). When it is corrected for contributions due to the reduction of the surface (≈ 20 J/mol per K [30]), liberation of the ligand water (22 J/mol per K), and the spin change of the iron (-9 J/mol per K), one has even a resulting $\Delta S \approx -310$ J/mol per K which has to be attributed to a change of the internal dynamics of the protein during the reaction.

Our model calculations are suited not for estimating differences of energy or enthalpy. They give, however, a good estimate for the loss of vibrational entropy of the ligand His E7 and the whole E-helix, $|\Delta S_E| < 40$ J/mol per K (cf. Table II). This value should be an upper bound for the reasons given above. It seems reasonable to assume that also the vibrational entropies of the much smaller and less directly involved heme and F-helix (see Fig. 3) will contribute even less to the total reaction entropy. A comparison with the experimental ΔS values shows that only 10–15% of this value can be explained by vibrational entropy contributions of the adjacent E-helix.

For the vibrational entropy in state A_1, e.g., we find $S_{vib} = 293$ J/mol per K. For a whole subunit (eight helices) S_{vib} should be in the range of 2–2.5 kJ/mol per K. This value confirms indeed the point of view, that a protein represents an enormous entropy reservoir [7,8] already with respect to the vibrational part of its entropy. However, only a small part of this vibrational entropy is available in the protein reaction. This is in good aggreement with the result [14] that even at denaturation of a protein the vibrational entropy is almost conserved. (The present reaction can be considered as 'first step in a reversible denaturation' [13].)

The considerable change of the geometry discussed above suggests that the local process of the internal binding reaction is coupled to (and influenced by) the entropy reservoir of global motions of parts of the protein and the large reaction entropy has its origin in fluctuations of tertiary or higher structure. For further discussions measurements and molecular dynamics simulation of isolated methemoglobin subunits are required. Work on this subject is in progress.

Acknowledgement

We would like to thank A. Metz and A. Kaes for preliminary calculations and measurements, U. Kallaß,

R. Seyfarth, S. Matussek and H. Lehky for technical assistance, and Ch. Bassaris for drawing assistance. Computer calculations were performed on a Cray Y-MP, computer graphics were done on an IRIS 4D25 workstation with INSIGHT/DISCOVER. We thank the HLRZ, Jülich, for computer time and Silicon Graphics, Köln, and Biosym, München, for the disposition of hardware and software.

Appendix A

A precise method for determining small changes of the optical extinction of solutions, in particular at temperature-jump experiments

Fig. 4 shows the scheme of a temperature-jump apparatus which differs from the usual device only by an additional resistor ΔR at the optical detector. Short-circuiting of this resistor by means of switch S delivers a calibration signal ΔE_{cal} which, for $\Delta E_{cal} \ll 1$, is given by

$$\Delta E_{cal} = \ln 10 \, \Delta R / R \tag{A.1}$$

The derivation of (A.1) is straightforward, taking into account that the current through the photodiode is essentialy independent of ΔR. At good signal-to-noise ratio, see Fig. 2, the experimental $\Delta E(t)$ is obviously measured with the same accuracy as the resistors. Therefore precise determination of thermodynamic data from temperature jump experiments is possible now.

Appendix B

Calculation of the vibrational entropy

The usual way to calculate quantum mechanically correct vibrational entropies is to diagonalize the Hessian of the potential energy and to use the resulting normal mode frequencies ω_i. Diagonalization is a way to transform to internal coordinates, the use of which enables one to express the classical approximation to the entropy by a determinant [23]. After deriving the general formalism we present here a method to calculate the classical approximation from a determinant without transformation to internal coordinates. Next we derive an approximative quantum mechanical correction in terms of a further determinant.

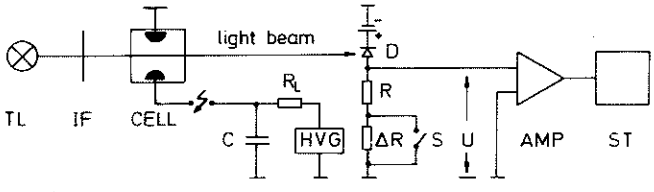

Fig. 4. Schematic drawing of the temperature jump apparatus. TL, tungsten lamp; IF, interference filter for selecting the optical wavelength used; Cell, T-jump cell; C, high voltage capacitor; HVG, high voltage generator; D, Photodiode BPW 34; AMP, amplifier; ST, digital storage. The switch S and the resistance ΔR serve for ΔE-calibrations (see text). Other optical parts are not shown.

1. Classical approximation

Let us consider a system of N atoms the configurations of which are given by vectors $\boldsymbol{r}$ containing the $3N$ cartesian coordinates. In the neighbourhood of a local minimum $\bar{\boldsymbol{r}}$ the potential $V(\bar{\boldsymbol{r}})$ can be represented by the second order approximation describing the vibrations about $\bar{\boldsymbol{r}}$,

$$V(\boldsymbol{r}) = V(\bar{\boldsymbol{r}}) + (\boldsymbol{r} - \bar{\boldsymbol{r}})^{\mathrm{T}} \boldsymbol{V} (\boldsymbol{r} - \bar{\boldsymbol{r}})/2 \tag{B.1}$$

where $\boldsymbol{V} = V(\bar{\boldsymbol{r}})$ is the $3N \times 3N$ Hessian matrix. For this harmonic potential all thermodynamic quantities can be expressed by the normal mode frequencies ω_i the squares of which are eigenvalues of the matrix

$$\boldsymbol{\Omega} = \boldsymbol{M}^{-1/2} \boldsymbol{V} \boldsymbol{M}^{-1/2} \tag{B.2}$$

where $\boldsymbol{M}$ is the diagonal mass matrix with diagonal elements $(m_1 \; m_1 m_1 \ldots m_N)$. With the abbreviation $\alpha_i = \hbar\omega_i / kT$ the quantum mechanical partition function reads

$$Q = \prod_i \sum_{n=0}^{\infty} \exp(-(n+1/2)\alpha_i) \tag{B.3}$$

The index i runs all modes with $\omega_i \neq 0$. As Q is a product of the contributions of all modes i, energy and entropy can be expressed as sums of the contributions from the single modes. For a particular mode the entropy (per mol) reads

$$S_i = R[\alpha_i / (\exp(\alpha) - 1) - \ln(1 - \exp(-\alpha_i))] \tag{B.4}$$

where R is the gas constant. Let us first consider the classical limit $0 < \hbar\omega \ll kT$ or $0 < \alpha \ll 1$ where B.4 takes the simple form

$$S_i^{cl} = R[1 - \ln \alpha_i] \tag{B.5}$$

which is readily summed up to give the complete classical vibrational entropy

$$\begin{aligned} S^{cl} &= \sum S_i^{cl} = R[3N - 0.5 \ln \textstyle\prod \alpha_i^2] \\ &= R[-0.5 \ln \det \boldsymbol{\Omega} + 3N \ln(kTe/\hbar)] \end{aligned} \tag{B.6}$$

Here e is the Euler number, $e = \exp(1)$. For the entropy difference between two substates 0 and 1 this finally leads to

$$\begin{aligned} \Delta S^{cl} &= S_1^{cl} - S_0^{cl} = -0.5 \, R \ln(\det \boldsymbol{\Omega}_1 / \det \boldsymbol{\Omega}_0) \\ &= 0.5 \, R \ln(\det \boldsymbol{V}_0 / \det \boldsymbol{V}_1) \end{aligned} \tag{B.7}$$

The crucial advantage of the classical approximation as compared with B.3 lies in the fact that only determinants have to be calculated, which reqires 5–10-times less computer time than the solution of the full eigenvalue problem for the calculation of the normal mode frequencies ω_i. However, as mentioned above the validity of B.7 is limited by conditions at either end of the spectrum and works well in practice only for frequencies in the range $0 < \hbar\omega < kT$, which makes direct application to molecules impossible. Zero frequencies associated with translation and rotation occur whenever free molecules are considered in cartesian coordinates, and can be avoided only by working with internal coordinates from the beginning or by discarding the corresponding terms after diagonalization of $\boldsymbol{\Omega}$. On the other hand, high frequency modes yield physically unreasonable negative entropies.

In the following we briefly describe a method to calculate the entropy approximately by using only determinants, i.e., without solving the eigenvalue problem or transforming to internal coordinates. The problem of zero frequencies is solved exactly, and the limit of high frequencies is treated by a suitable approximation. The final approximation covers the whole frequency range and requires only twice the computing time of the classical approximation.

2. Classical approximation for free molecules

A free nonlinear molecule has six linearly independent improper normal modes of vanishing frequency connected with unhindred translation and rotation of the whole molecule. The normal mode vectors span a six-dimensional subspace and are eigenvectors of the matrix Ω with vanishing eigenvalues. Let us now define a projector Π_6 onto this subspace. As the vectors are also eigenvectors of the projector with unit eigenvalues, the modified matrix

$$\boldsymbol{\Omega}' = \boldsymbol{\Omega} + \Pi_6 \tag{B.8}$$

will possess exactly the same eigenvectors and spectrum as before exept for the six zero eigenvalues which now have been replaced by 1. Hence, if $\boldsymbol{\Omega}'$ is inserted instead of $\boldsymbol{\Omega}$ in B.7, the improper modes do not contribute to the entropy difference and the classical approximation holds. By the same argument one can define a modified Hessian with a projector $\boldsymbol{P}_6$,

$$\boldsymbol{V}' = \boldsymbol{V} + \boldsymbol{P}_6 \tag{B.9}$$

and write the classical approximation as

$$\Delta S^{\mathrm{cl}} = 0.5\, R \ln(\det V_0'/\det V_1') \tag{B.10}$$

which now holds also for a free molecule. For structuring the projector $\boldsymbol{P}_6$ for either substate, one finds from general considerations the following eigenvectors of V connected with translation and rotation,

$$\begin{aligned}
\boldsymbol{a}_1 &= (1\,0\,0\,1\,0\,0\ldots 0)^{\mathrm{T}} \\
\boldsymbol{a}_2 &= (0\,1\,0\,0\,1\,0\ldots 0)^{\mathrm{T}} \\
\boldsymbol{a}_3 &= (0\,0\,1\,0\,0\,1\ldots 1)^{\mathrm{T}} \\
\boldsymbol{a}_4 &= \left(0, -\bar{z}_1, \bar{y}_1, 0, -\bar{z}_2, \bar{y}_2, \ldots \bar{y}_N\right)^{\mathrm{T}} \\
\boldsymbol{a}_5 &= \left(\bar{z}_1, 0, -\bar{x}_1, \bar{z}_2, 0, -\bar{x}_2, \ldots \bar{x}_N\right)^{\mathrm{T}} \\
\boldsymbol{a}_6 &= \left(-\bar{y}_1, \bar{x}_1, 0, -\bar{y}_2, \bar{x}_2, 0, \ldots 0\right)^{\mathrm{T}}
\end{aligned} \tag{B.11}$$

which can be shown to have eigenvalues zero and are given here without proof. By orthogonalizing the a_i and normalizing the resulting vectors, one obtains six unit vectors e_i and a projector

$$\boldsymbol{P}_6 = \sum \boldsymbol{e}_i \boldsymbol{e}_i^{\mathrm{T}} \tag{B.12}$$

3. Quantum mechanical correction

The classical approximation for the entropy of a single mode B.5 fails to give zero in the limit of high frequencies and becomes more and more negative instead. We hence introduce the approximation

$$S_i' \sim 0.5\, R \ln\left((\alpha_i^2 + e^2)/\alpha_i^2\right) \tag{B.13}$$

with $e = \exp(1)$. This function obviously tends to the classical limit at small α and vanishes at large α as it must do. Numerical investigations show that it is a good approximation to the correct function B.4, S' being slightly greater for all α. Because of the special form, the sum over all modes is easily expressed by two determinants,

$$\begin{aligned}
S' \sim \sum S_i' &= 0.5\, R \ln\left(\det(\hbar/kT)^2 \boldsymbol{\Omega} + e^2 \mathbf{1}\right)/\det\left((\hbar/kT)^2 \boldsymbol{\Omega}\right) \\
&= -0.5\, R \ln(\det V) + 0.5 \ln\left(\det\left(\boldsymbol{V} + (kTe/\hbar)^2 \boldsymbol{M}\right)\right)
\end{aligned} \tag{B.14}$$

While the first part is essentially the classical approximation, the second term represents a quantum mechanical correction. For the entropy difference between two states of the same molecule one thus obtains

$$\begin{aligned}
\Delta S' = \Delta S^{\mathrm{cl}} &+ 0.5\, R \ln\left(\det\left(V_1 + (kTe/\hbar)^2 \boldsymbol{M}\right)\right. \\
&\left./\det\left(\boldsymbol{V}_0 + (kTe/\hbar)^2 \boldsymbol{M}\right)\right)
\end{aligned} \tag{B.15}$$

With ΔS^{cl} from (B.10) this is finally the expression used in this work.

References

1 Reif, F. (1985) Statistische Physik und Theory der Wärme, Walter de Gruyter, Berlin, New York.

2 Perutz, M.F. (1979) Annu. Rev. Biochem. 48, 327–386.

3 Frauenfelder, H., Petsko, G.A. and Tsernoglou, D. (1979) Nature 280, 558–563.
4 Austin, R.H., Beeson, K.W., Eisenstein, L., Frauenfelder, H. and Gunsalus, I.C. (1975) Biochemistry 14, 5355–5373.
5 Iben, I.E.T., Braunstein, D., Doster, W., Frauenfelder, H., Gong, M.K., Johnson, J.B., Luck, S., Ormos, P. Schulte, A., Steinbach, P.I., Xie, A.H. and Young, R.D. (1989) Phys. Rev. Lett. 62, 1916–1919.
6 Steinhoff, H.J. (1990) Eur. Biophys. J. 18, 57–62.
7 Koshland, D.F. jr. (1960) Adv. Enzymol. 22, 45.
8 Westheimer, F.H. (1962) Adv. Enzymol. 24, 441–482.
9 Brooks, B.R. and Karplus, M. (1983) Proc. Natl. Acad. Sci. USA 80, 6571–6575.
10 Page, M.I. and Jencks, W.P. (1971) Proc. Natl. Acad. Sci. USA 68, 1678–1683.
11 Moore, W.J. (1972) Physical Chemistry, Prentice-Hall, Englewood Cliffs, N.J.
12 Parak, F. and Knapp, E.W. (1984) Proc. Natl. Acad. Sci. USA 81, 7088–7092.
13 Doster, W., Cusak, S. and Petry, W. (1989) Nature 337, 754–756.
14 Karplus, M., Ichiye, T. and Pettitt, B.M. (1987) Biophys. J. 52, 1083–1085.
15 Elber, R. and Karplus, M. (1987) Science 235, 318–321.
16 Bracht, A., Eufinger, B.R., Redhardt, A., and Schlitter, J. (1979) Biochem. Biophys. Res. Commun. 86, 585–593.
17 Bracht, A., Eufinger, B.R., Neumann, H.J., Niephaus, G., Redhardt, A., and Schlitter, J. (1980) FEBS Lett. 114, 157–160.
18 Dreyer, U. and Ilgenfritz, G. (1979) Biochem. Biophys. Res. Commun. 87, 1011–1017.
19 Page, M.I. and Williams, A. (1987) Enzyme Mechanisms, Royal Society of Chemistry, London.
20 Benesch, R.E., Benesch, R., Renthal, R.D. and Maeda, N. (1972) Biochemistry 11, 3576–3582.
21 Bernasconi, C.F. (1976) Relaxation Kinetics, Academic Press, London.
22 van Gunsteren, W.F. and Berendsen, H.J.C. (1987) Biomos. Groningen.
23 Schlitter, J. and Metz, A. (1988) Int. J. Comp. Math. 24, 65–71.
24 Ladner, R.C., Heidner, E.J. and Perutz, M.F. (1977) J. Mol. Biol. 114, 385–414.
25 Karplus, M. and Kushik, J.N. (1981) Macromolecules 14, 325–332.
26 Steinhoff, H.J., Lieutenant, K., and Redhardt, A. (1989) Biochim. Biophys. Acta 996, 49–56.
27 Steinhoff, H.J. (1985) Dissertation, Ruhr-Universität Bochum, 4630 Bochum, Germany.
28 Eaton, W.A. and Hochstrasser, R.M. (1968) J. Chem. Phys. 49, 985–995.
29 Eigen, M. and de Maeyer, L. (1963) in Technique of Organic Chemistry (de Friess, S.L., Lewis, E.S. and Weissberger, A., eds.), Vol. 8, Part II, 2nd Edn., pp. 895–1054, Interscience, New York.
30 Chothia, C. (1974) Nature 248, 338–339.
31 Tomoda, A., Sugimato, K., Suhara, M., Takeshita, M. and Yonegama, Y. (1978) Biochem. J. 171, 329–335.